Eur Biophys J (2001) 30: 129–139
DOI 10.1007/s002490000117

ARTICLE

**Marisa Huertas de la Torre · Riccardo Forni
Giuseppe Chirico**

Brownian dynamics simulations of fluorescence fluctuation spectroscopy

Received: 10 July 2000 / Revised version: 12 October 2000 / Accepted: 13 October 2000 / Published online: 19 January 2001

Abstract We have developed a program for the simulation of the fluorescence fluctuations as detected from highly diluted samples of (bio)molecules. The model is applied to translational diffusion and takes into account the hydrodynamic interactions. The solution concentration is kept constant by assuming periodic boundary conditions and spans here the range $0.5 < C < 10$ nM. We show that the fluorescence correlation functions can be accurately computed on systems of limited size (a few molecules per simulation box) by simulating for a total time ~100–300 times the diffusion relaxation time of the fluorescence autocorrelation function. The model is applied also to the simulation of the scanning fluorescence correlation spectroscopy (FCS) and of the photon counting histograms for the confocal collection configuration. Scanning FCS simulations of highly diluted samples ($C \approx 0.5$ nM) show anticorrelation effects in the autocorrelation functions of the fluorescence signal that are less evident for higher concentrations. We suggest here that this effect may be due to the non-uniform occupancy of the scanning area by the fluorophores.

Keywords Fluorescence correlations · Brownian dynamics · Photon counting · Autocorrelation functions · Scanning fluorescence correlation spectroscopy

Introduction

Fluorescence correlation spectroscopy (FCS) has been widely applied to the investigation of highly dilute biological samples. It allows detection of tiny amounts of fluorescent molecules and to assess the degree of their aggregation (Quian and Elson 1990) and interactions (Schwille et al. 1997; Kask et al. 2000) by directly counting them in solution (Chen at al. 1999; Kask et al. 1999). This feature is based on the possibility of measuring accurately the fluorescence fluctuations, correcting them for the possible contribution from uncorrelated background, shot noise and triplet states (Widengren et al. 1995). A second parallel method for counting the fluorescent particles in dilute solutions is based on the computation of the photon-counting histograms (Chen et al. 1999; Muller et al. 2000). In all these cases, analytical models have been developed and simple expressions are available to describe the trend of the experimental data.

However, the study of a number of phenomena by fluorescence fluctuation spectroscopy can take relevant advantage from the use of numerical simulations. The analysis of fluorescence data for the study of molecular photo-dynamics and interactions can be improved by refined theoretical treatments based also on numerical simulations. Moreover, recent developments in microscopy have led to increasing spatial resolution (of the order of 300 nm) that is now comparable with the size of some biological molecules such as small plasmid DNAs or large protein systems. The fluorescence fluctuations arising from the diffusional motion of single macromolecules in the beam spot are difficult to predict with analytical models and the numerical simulations are expected to help substantially in the treatment of the spectroscopic data. In order to exploit the potentiality of the numerical simulations in this research, a preliminary study of the limitations and the specific requirements for the study of the fluorescence fluctuations must be performed.

The aim of the present communication is the description and test of a program for the Brownian dynamics simulation of fluorescence fluctuation spectroscopy in highly dilute solutions of small macromolecules such as globular proteins. We discuss the requirements for obtaining sensible simulations of the

M. Huertas de la Torre · R. Forni · G. Chirico (✉)
Istituto Nazionale per la Fisica della Materia,
Dipartimento di Fisica G. Occhialini,
Università di Milano Bicocca, Via Celoria 16,
20133 Milan, Italy
Fax: +39-02-2392482

autocorrelation functions also by comparing the classical FCS to the scanning FCS method. The protocol for the simulation procedure of the photon counting histogram is also outlined and applied. We further show that fluorescence correlation measurements with scanning methods in highly dilute solutions or on single molecules may lead to definite anticorrelations in the correlation function when observed for short times of ~10 times the diffusion time of the macromolecules in the excitation volume. We speculate on the possibility that these anticorrelation features could be exploited for the investigation of the structure of macromolecules of the size of the laser beam waist.

Description of the model

Brownian dynamics model

We treat the case of small globular proteins whose translational frictional properties can be simulated by beads with radius a. We allow for different sizes of the proteins with a_i indicating the radius of the ith protein. The simulation of the dynamics of a solution at molar concentration C is performed in a cube of side L_{box} by choosing the number of simulated proteins N in the box such that $C = N/(L^3_{box}N_{av})$, where N_{av} is the Avogadro number. The solvent is considered as a continuum with an effective viscosity, η, that is assumed to be uniform within the system. Periodic boundary conditions are then applied in order to avoid surface effects (Allen and Tildesley 1987). The box is replicated throughout the space to create an infinite grid and every time a particle overpasses one of the boundaries, one of its periodic images will enter from the opposite face. The solution density is kept constant by assuming periodic boundary conditions. Since most of the time the concentration of protein solutions are given in terms of mass concentration, c, it is useful to link this quantity to the box size:

$$c = \frac{M_{tot}}{V} = \frac{Nm_{mon}}{V} = \frac{N(v_{mon}\rho_{mon})}{V} = \frac{N(4/3\pi a^3)\rho_{mon}}{L^3_{box}} \tag{1}$$

where N is the number of monomers within the box and m_{mon}, v_{mon} and ρ_{mon} the mass, volume and density of the protein, respectively. The side of the box is then determined according to the density.

On each bead we assume a local frame of reference whose three unitary and orthogonal vectors are $\{\mathbf{f}, \mathbf{v}, \mathbf{u}\}$ and have their origin at the center of mass of the bead. At each simulation step the configuration of the system is given by the N coordinates, $\mathbf{r}_j$, of the center of mass of the beads and $2N$ unitary vectors, $\mathbf{f}_j$ and $\mathbf{u}_j$. Regarding inter-protein interactions, only the screened electrostatic interaction due to the charge surface density on the proteins at the specific experimental pH value is considered. The force on the jth protein due to the interaction with the ith protein, each endowed with charge Q_i and Q_j, is given by:

$$\mathbf{F}_{ji} = -\mathbf{F}_{ij} = \frac{Q_iQ_j\exp\left[k_D(a_i + a_j - R_{ij})\right]}{\varepsilon(1 + k_Da_i)(1 + k_Da_j)}\left(\frac{k_DR_{ij} + 1}{R^2_{ij}}\right)\mathbf{U}_{ij} \tag{2}$$

where $\mathbf{R}_{ij} = \mathbf{r}_j - \mathbf{r}_i$, $R_{ij} = |\mathbf{R}_{ij}|$ and $\mathbf{U}_{ji} = \mathbf{R}_{ij}/R_{ij}$. The dielectric constant of the medium is ϵ and the screening Debye-Hückel parameter is $k_D = (8\pi L_BC)^{0.5}$, where L_B is the Bjerrum length (Dhont 1996). As a reference, $L_B \approx 0.73$ nm in water at 25 °C. The total force $\mathbf{F}_j$ acting on the jth protein is the sum of all the forces due to the interaction with the other proteins. In the computation of the force we have assumed the minimum image convention algorithm (Allen and Tildesley 1987) by computing the forces between the jth protein and other proteins (or images of them in the neighboring boxes) in a box of length L_{box} centered around the jth protein.

In order to keep the simulation CPU time at a minimum, we have also applied the cut-off approximation, that is, only interaction between spheres closer than the cut-off distance, $\mathbf{r}_c$, will be considered. In this case, and using a circular cut-off, the number of interaction terms to be calculated is reduced by a factor of $4\pi {r_c}^3/3{L^3}_{box}$, so the CPU time clearly diminishes.

The Brownian dynamics (BD) is performed according to the standard algorithm by Ermak and McCammon (1978) for the translation and its extension to rotational diffusion (Dickinson et al. 1985). The translational diffusion $3N \times 3N$ matrix is computed according to the Rotne-Prager-Yamakawa tensor (Rotne and Prager 1969; Yamakawa 1970). For the diagonal terms, the 3×3 matrices are diagonal with the non-zero terms $D_0 = KT/6\pi\eta a$. For the off-diagonal matrices ($i \neq j$):

$$\mathbf{D}_{ij} = \frac{KT}{8\pi\eta R_{ij}}\left[\left(\mathbf{I} + \frac{\mathbf{R}_{ij} : \mathbf{R}_{ij}}{R^2_{ij}}\right) + \frac{2a^2}{R^2_{ij}}\left(\frac{1}{3}\mathbf{I} - \frac{\mathbf{R}_{ij} : \mathbf{R}_{ij}}{R^2_{ij}}\right)\right] \tag{3}$$

where η is the solution viscosity, a is the sphere radius, $\mathbf{R}_{ij}$ is the vector from the center of the of sphere i to the center of sphere j, and $\mathbf{I}$ is the unit tensor.

It should be noted that when overlapping occurs, there can be problems when inverting the supermatrix in the frictional force calculation (Carrasco et al. 1999). Therefore when the overlapping occurs we have chosen the diffusion tensor proposed, on the basis of empirical considerations, by Zipper and Durchschlag (1997):

$$\mathbf{D}_{ij} = \frac{KT}{6\pi\eta a}\left[\left(1 - \frac{9}{32}\frac{R_{ij}}{a}\right)\mathbf{I} + \frac{3}{32}\frac{\mathbf{R}_{ij} : \mathbf{R}_{ij}}{R_{ij}a}\right] \tag{4}$$

As this tensor refers to the penetration of equal size spheres, these authors assume a mean radius between the two particles. There are two possibilities:

$$a_{mean} = (a_i + a_j)/2 \tag{5}$$

$$a_{\text{mean}} = \left[\left(a_i^3 + a_i^3\right)/2\right]^{1/3} \tag{6}$$

These are empirical solutions with no clear theoretical support, but lead to acceptable results and allow us to solve the inversion problem of the supermatrix in the frictional force calculations.

For the rotational diffusion, we neglect rotational hydrodynamic interactions and assume that the rotational diffusion for the ith protein is described by two diffusion coefficients, one for spinning $\Theta_{\text{S},i}$ and one for tumbling $\Theta_{\text{T},i}$ motions.

In the BD algorithm of Ermak-McCammon (Ermak and McCammon 1978), the position of the beads $\mathbf{r}_i$ after the time step δt are obtained from the previous ones, $\mathbf{r}_i^0$, accordingly to:

$$\mathbf{r}_i = \mathbf{r}_i^0 + \sum_{j=1}^{N} \frac{\partial \mathbf{D}_{ij}^0}{\partial \mathbf{r}_i}\delta t + \frac{1}{kT}\sum_{j=1}^{N} \mathbf{D}_{ij}^0 \cdot \mathbf{F}_j^0 \delta t + \mathscr{R}_i(\delta t) \tag{7}$$

where the superscript 0 indicates that the variable is to be evaluated at the beginning of the Brownian step; $\mathbf{F}_j$ is the mechanical force on bead i, $\mathbf{D}_{ij}$ the diffusion tensor and $\mathscr{R}_i(\delta t)$, the random vector.

This stochastic term is sampled from a Gaussian distribution defined by:

$$\langle \mathscr{R}_i(\delta t) \rangle = 0 \tag{8}$$

$$\left\langle \mathscr{R}_i(\delta t)\mathscr{R}_j(\delta t) \right\rangle = 2\mathbf{D}_{ij}(t)\delta t \tag{9}$$

The diffusion tensors used here (Eqs. 3 and 4) have the property that:

$$\sum_{j=1}^{N} \frac{\partial \mathbf{D}_{ij}^0}{\partial \mathbf{r}_i} = 0$$

and therefore this term can be dropped from Eq. (7). This greatly simplifies the calculation of the displacements as the gradient of the diffusion tensor does not have to be calculated. The BD algorithm simplifies to:

$$\mathbf{r}_i = \mathbf{r}_i^0 + \frac{1}{kT}\sum_{j=1}^{N} \mathbf{D}_{ij}^0 \cdot \mathbf{F}_j^0 \delta t + \mathscr{R}_i(\delta t) \tag{10}$$

We give here also the extension of the previous algorithm to the study of rotational motion even though we are not applying numerically this algorithm in the present report. For the rotational motion we assume that no external torques are acting on the proteins, i.e. no dipole moments on the proteins are considered. In this case, for each simulation step the unitary vectors change their direction according to:

$$\begin{aligned} \mathbf{f}_i(t+\delta t) &= \mathbf{f}_i(t) + \delta\phi_{\text{S},i}\mathbf{v}_i(t) - \delta\phi_{\text{T},i}\mathbf{u}_i(t) \\ \mathbf{u}_i(t+\delta t) &= \mathbf{u}_i(t) + \delta\phi_{\text{T},i}\mathbf{f}_i(t) + \delta\phi_{\text{T},i}\mathbf{v}_i(t) \end{aligned} \tag{11}$$

where the stochastic terms are sampled from Gaussian distributions defined by:

$$\begin{aligned} \left\langle \delta\phi_{\text{S},i}\delta\phi_{\text{S},j} \right\rangle &= 2\delta_{ij}\delta t\Theta_{\text{S},i} \\ \left\langle \delta\phi_{\text{T},i}\delta\phi_{\text{T},j} \right\rangle &= 2\delta_{ij}\delta t\Theta_{\text{T},i} \end{aligned} \tag{12}$$

A critical parameter in our simulations is the time step. On the one hand, its size is restricted to values which are sufficiently high so that we are on a diffusive regime ($\Delta t \gg m\mathbf{D}_{ii}^0/kT$). On the other hand, numerical accuracy limits its maximum value, requiring it to be sufficiently low so that the force on the particles and the diffusion tensor are essentially constant during the time step (Iniesta and Garcia de la Torre 1990).

Computation of the fluorescence fluctuations

Fluorescence fluctuations arise from the diffusional motion of the small globular proteins in and out of the excitation volume. The excitation of tiny volumes of solution is obtained either from the use of confocal microscopy (Wilson 1990) or of multiphoton excitation microscopy (So et al. 1995).

In the present communication we assume that in the sample region there is only one fluorescent chemical species and that only a single photon emitted by the light source is needed in order to excite a fluorescent molecule. In this case, the fluorescence emitted by the sample is:

$$F(t) = kQG(\Omega(t)) \int W(\mathbf{r}) \cdot n(\mathbf{r},t)\mathrm{d}\mathbf{r} \tag{13}$$

In this equation, k is a numerical constant, $n(\mathbf{r},t)$ is the number concentration at position $\mathbf{r}$ at time t, Q is the absorption cross-section, $W(\mathbf{r})$ is called the molecular detection efficiency (MDE) and $G(\Omega(t))$ is the photoselection factor that depends on the orientation of the excitation and the emission dipoles, μ^{exc} and μ^{em}, with respect with the excitation and emission polarization direction, ϵ_{exc} and ϵ_{em}:

$$G(\Omega(t)) = f_{\text{E}}(\Omega(t))f_{\text{A}}(\Omega(t)) \tag{14}$$

where the excitation and the emission factors are: $f_{\text{A}}(\Omega(t)) = \left[\mu^{\text{exc}}(\Omega(t)) \cdot \varepsilon_{\text{exc}}\right]^2$ and $f_{\text{E}}(\Omega(t)) = \left[\mu^{\text{em}}(\Omega(t)) \cdot \varepsilon_{\text{em}}\right]^2$.

In the case of confocal single photon microscopy, the use of high numerical aperture objectives (NA $\approx$ 1) and small detection pin-holes ($\sim$100 μm in diameter) leads to an excitation laser profile well described by a 3-D Gaussian:

$$W(r) = I_0 \exp\left[-2\frac{(x^2+y^2)}{w_0^2} - 2\frac{z^2}{z_0^2}\right] \tag{15}$$

with w_0 and z_0 being the transversal and longitudinal width, respectively (Rigler et al. 1993).

In our case, the numerical concentration $n(\mathbf{r},t)$, is a discrete quantity because the system is made of N particles:

$$n(\mathbf{r},t) = \sum_{i=1}^{N} \delta(\mathbf{r} - \mathbf{r}_i(t)) \tag{16}$$

The fluorescent signal becomes:

$$F(t) = kQI_0 \sum_{i=1}^{N} G(\Omega_i(t)) \times \exp\left[-2\frac{\left[(x-x_L)^2+(y-y_L)^2\right]}{w_0^2} - 2\frac{(z-z_L)^2}{z_0^2}\right] \quad (17)$$

where (x_L,y_L,z_L) is the position vector of the laser beam.

In the case when unpolarized excitation is used and no analyzer is employed for the detection, the fluorescence signal does not depend on the orientations of the transition dipoles since the orientation factor in Eq. (17) is rotationally averaged. In the following we will not take into account the orientation factors, though the computation of the correlation functions can easily be performed within our model and is essential in the case of simulations of macromolecules of sizes similar to the excitation spots.

Simulation methods

We represent the model proteins with spheres of radius 8.57×10^{-8} cm, having a density = 0.75 g/cm^3 and a charge of Q in the range 1–5 proton charge. This equates approximately to a small globular polypeptide with molecular weight 1600 Daltons corresponding to ~20 residues.

In all of our FCS simulations we have used a number of particles $6 \leq N \leq 12$ and excitation volumes which range from 0.18 to 2.1 fL that correspond to $w_0 \approx 0.35$–0.5 μm and $z_0 \approx 1.5$–3 μm. In all our FCS simulations we have positioned the beam laser in the center of the box. Typical mass concentrations are chosen in the interval $c = 0.8$–16 μg/L, which correspond to molarities of $C = 0.5$–10 nM. In these conditions there is a minimum of 0.05 and a maximum of 12 particles per excitation volume.

We consider the solvent as a continuum, having a density of 1 cP and a dielectric constant $\epsilon = 80$. The solution has a high ionic strength (50–100 mM) and the temperature of the system is uniform and equal to 293 K. At the beginning of each simulation we put the beads in such a way that there is one of them at the center of each cube of volume L_{box}^3/N in which we can divide the total volume of the box. We run then 10^6 equilibration steps before starting the simulation of interest. Unless specified, the length of the trajectories is 210 ms and the time step is 200 ps.

Results

Translational diffusion

As a first test of the computer simulations, we have measured the protein's diffusion coefficient from the slope of the center-of-mass mean-square displacement, according to the relation $\langle|\mathbf{r}_i(t) - \mathbf{r}_i(0)|^2\rangle = 6D_i\delta t$. In order to obtain the correct diffusion relation, one must carefully avoid even rare overlapping of the beads. When no care is taken of avoiding this overlapping, a noticeable dependence of the protein translational diffusional coefficient on the number of particles present in solution, N, is found as shown in Fig. 1. This behavior cannot be ascribed to protein–protein interactions because we are working with a very dilute solution having high ionic strength (50–100 mM) and low particle charges. Besides, the side of the cube, L_{box}, is chosen so that the numerical density is kept constant when varying the number of particles. The reason for this anomalous behavior is only the partial overlapping between beads, which takes place when by random displacement the distance between two of them is less than the sum of their respective radii.

The overlapping can be solved in two different ways. The forces can be cut-off, if two beads overlap, at the value assumed when they are at the distance of maximum approach. A second possibility is to compute again the random term in the BD algorithm until no overlapping occurs. This procedure is based on the consideration that the random displacement is the dominant part of the total protein displacement. For the simulations presented here, where low surface charge densities

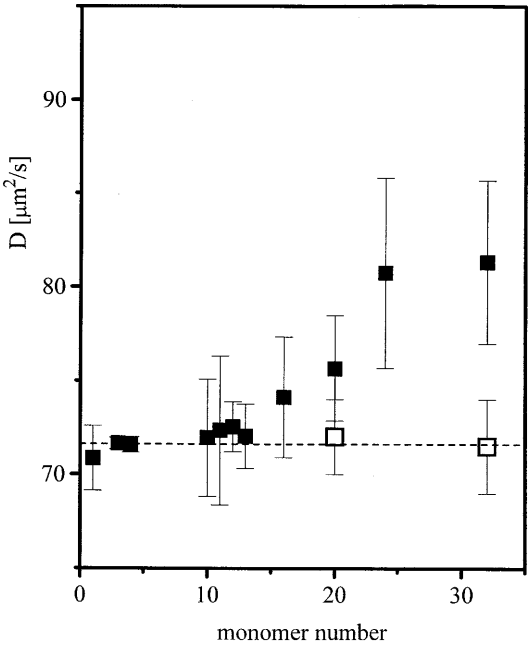

Fig. 1 Diffusion coefficient of the proteins obtained from the slope of the center of mass displacement. The simulations were run with $Q = 1$, ionic strength = 50 mM. The number of proteins N is varied as indicated in the plot, while the solution concentration is kept constant at $c = 10$ μg/L by varying the box size. Each diffusion coefficient value is obtained as an average over the N monomers employed for the simulation. The *dashed line* corresponds to the simulation value of $D = 71.4$ μm^2/s. The two *open squares* have been obtained by re-computing the random displacement at each time step until no overlap was found

are considered and relatively high screening is assumed, the two methods give very similar results and the first has the advantage of requiring less CPU time. However, when stronger interactions are considered the second solution should be preferred.

Since we are changing the box length and the number of molecules in order to obtain a constant value of the concentration, we cannot ascertain from the results reported in Fig. 1 whether the boundary conditions, related to the size of the box, or the overlapping effect is responsible for the observed behavior. We have therefore performed simulations with the second type of corrections suggested above and show the corresponding diffusion coefficients for $N=20$ and $N=32$ in Fig. 1 as open squares. As was expected, the computed diffusion coefficient is now very close to the expected value.

An additional critical parameter in our simulations is the time step. We are interested in values of Δt as high as possible in order to reach longer trajectories (always in the diffusive regime, that is $\Delta t \gg \tau_{ij} = m_j D_{ij}/kT$). On the other hand, its value must guarantee that the change of the potential energy per particle is less than kT and that the diffusion tensors are constant during the time step. Since the numerical integration algorithm is accurate for $\Delta t \to 0$ (Iniesta and Garcia de la Torre 1990), we must find a range of time step values where the algorithm is stable and the diffusive regime is ensured. Figure 2 shows the dependence of the translational diffusion coefficient on the time step that we find for the case $Q=5$ and for an ionic strength of 50 mM. Instead of remaining constant with Δt, there is a gradually growth of the diffusion coefficient when the time step overcomes a certain value. For large Δt values a particle may get too close to another one in just one step, giving rise to a repulsion higher than that predicted by the dynamics equations. The particle then moves more rapidly than expected from the stochastic equations and this leads to a higher effective translational diffusion coefficient. Based on the results in Fig. 2, we have decided to use a value of 200 ps for the time step.

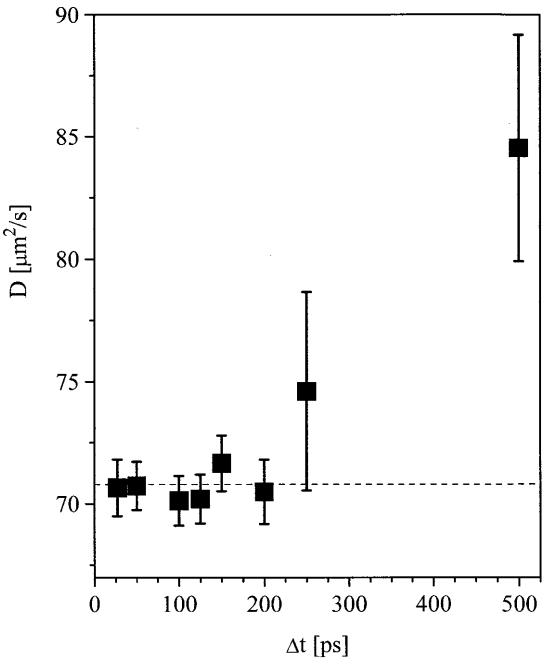

Fig. 2 Diffusion coefficient of the proteins obtained from the slope of the center of mass displacement reported versus the time step of the simulation. The simulations where run with $Q=5$, ionic strength = 50 mM. The concentration is $c=10$ μg/L and $N=10$. Each diffusion coefficient value is obtained as an average over the monomers employed for the simulation. The *dashed line* corresponds to the simulation value of $D=71.4$ μm^2/s

Fluorescence correlation spectroscopy

The autocorrelation function of the fluorescence fluctuations gives information on the dynamics of the system and is defined as:

$$G(\tau) = \frac{\langle \delta F(t+\tau) \cdot \delta F(t) \rangle_t}{\langle F(t) \rangle_t^2} \tag{18}$$

where $\delta F(t) = F(t) - \langle F \rangle$ is the fluctuation around the average fluorescence intensity and the subscript "t" indicates the average over the time. If the particles undergo only translational diffusion, the fluorescence fluctuations occur because the particles sample different portions of the laser beam in their Brownian motion and $G(\tau)$ becomes:

$$G(\tau) = \frac{\gamma}{\langle N \rangle} \cdot \frac{1}{(1+\tau/\tau_{xy}) \cdot (1+\tau/\tau_z)^{1/2}} \tag{19}$$

where $\gamma = (1/2)^{3/2}$ is a geometric constant for the 3-D Gaussian approximation and $\langle N \rangle$ is the average number of molecules in the sample region related to the average number concentration, $\langle n \rangle$, as:

$$\langle N \rangle = \langle n \rangle V_{\mathrm{EXC}} \tag{20}$$

The excitation volume for the 3-D Gaussian approximation is $V_{EXC} = (\pi/2)^{1.5} w_0^2 z_0$ and τ_{xy} and τ_z are the characteristic diffusion times of the particle through the area illuminated by the focused laser beam in the transversal and longitudinal directions, respectively. The $G(\tau)$ dependence on τ_z is weaker than that on τ_{xy}, and it is more evident at longer times:

$$\tau_{xy} = \tau_{\mathrm{d}} = w_0^2/4D \tag{21}$$

$$\tau_z = z_0^2/4D \tag{22}$$

As we have commented before, we use a time step of 200 ps, which is much greater than the momentum relaxation time, $\tau \approx 0.1$ ps. For our choice of the protein size, the diffusion coefficient is $D=71.4$ μm^2/s and the typical diffusion time is $\tau_{xy} \approx 0.56$ ms for $w_0=0.4$ μm.

The total simulation time, 210 ms, is much larger (~375 times) than the diffusion time.

In Fig. 3 we show a typical graph of the fluorescence light impinging on the detector as a function of time. This quantity does not represent the output of the detector that contains also the effect of the shot noise. Apart from the first channel, $G(0)$, no other shot noise effect is present in the autocorrelation function. However, if we liked to simulate the histogram of the photon counting as obtained from the photo-detector, we should convolute the simulated fluorescence with the Poisson response of the detector, as outlined later in this discussion.

From each BD trajectory we have computed the fluorescence correlations with different laser parameters for our simulations in the following intervals, $w_0 = 0.35$–$0.75\,\mu m$ and $z_0 = 1.75$–$3.75\,\mu m$, so that the 3-D Gaussian approximation is still valid for the laser intensity profile in confocal collection. An example of the autocorrelation function of the fluorescence is represented in Fig. 4 for a solution at $c \approx 3\ \mu g/L$, together with a best fit according to Eq. (19). In the best fit procedure the relaxation time in the axial direction has been assumed as $\tau_z = \tau_{xy}(z_0/w_0)^2$. The uncertainties reported in Fig. 4 are obtained dividing the 210 ms trajectory into four equal-size subtrajectories (52.5 ms each), on which we have computed the fluorescence autocorrelation function and have averaged the result.

The diffusion time τ_d is a function of w_0 and of the translational diffusion coefficient, D, which is obtained from the position correlation functions with an error $\leq 2\%$. Representing τ_d (obtained from the fit of the autocorrelation function) versus the ratio w_0^2/D, a linear dependence with a slope 0.26 ± 0.03 is found, as is expected from Eq. (21).

We have not explicitly added additional noise to the simulated autocorrelation functions in the results presented below. However, one must take into account the dependence of the normalized standard deviation $\mathrm{CFSD}(\tau) = \langle G(t)\rangle(\langle G(t)^2\rangle - \langle G(t)\rangle^2)^{-0.5}$ on three parameters: the number of photons emitted per molecule and per sampling time, N_p, the total number of samplings M_s per measurement, and the number of molecules per excitation volume, μ. In Quian's treatment (Quian 1990) the CFSD(0) scales as:

$$\mathrm{CFSD}(0) \to N_p \left(\frac{M}{1 + N_p^2} \right)^{0.5} \quad \text{for } \mu \to \infty \tag{23}$$

which is similar to the result of Koppel (1974), and:

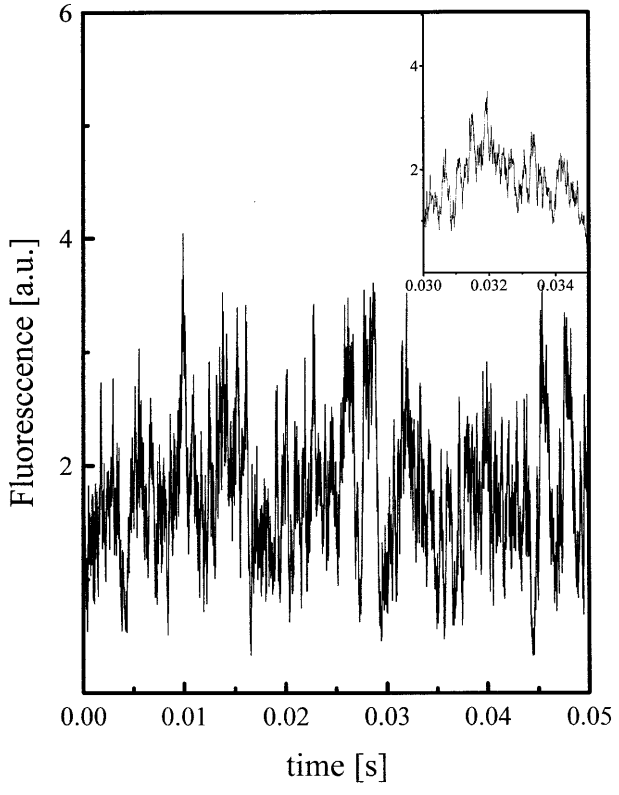

Fig. 3 Fluorescence signal simulated from a solution of proteins at a concentration $c = 3\ \mu g/L$. The number of monomers per cell is $N = 10$, the ionic strength is 50 mM and $Q = 1$. The *inset* shows an enlargement of the fluorescence rate between 30 ms and 32 ms of simulation time

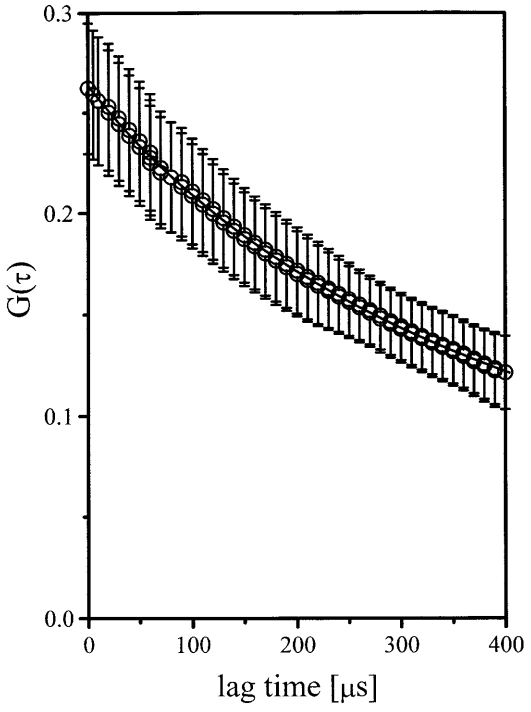

Fig. 4 Fluorescence autocorrelation function $G(\tau)$ for the case reported in Fig. 3 and for $w_0 = 0.35\ \mu m$ and $z_0 = 1.75\ \mu m$, corresponding to $V_{EXC} = 0.42$ fL. The *solid line* is the best fit to Eq. (19) with best fit parameters, $\tau_{xy} = 470 \pm 100\ \mu s$ and $\langle N\rangle = 0.9 \pm 0.14$. The relaxation time for the diffusion in the axial direction is assumed as $\tau_z = \tau_{xy}(z_0/w_0)^2$ in the best fit procedure. The uncertainties correspond to the average over four subtrajectories of the original 210 ms trajectory

$$\mathrm{CFSD}(0) \rightarrow N_\mathrm{p}\left(\frac{\mu M}{1+N_\mathrm{l}^2}\right) \quad \text{for } \mu \rightarrow 0 \tag{24}$$

which, differently from the Koppel result (Koppel 1974), depends on the number of molecules per excitation volume. Therefore the higher is the dilution, $\mu \approx 0$, the longer should be the measurements and the duration time scales approximately as $C^{-0.5}$. Finally, it must be noticed that an extremely important parameter is the molecular brightness that determines the CFSD(0) linearly through N_p. The simulations presented here are for normalized fluorescence properties and are not meant to reproduce the behavior of the standard deviation of the $G(\tau)$ given by Eqs. (23) and (24).

Photon counting histograms

If we are interested in the spectroscopic heterogeneity of the sample, it is more convenient to analyze the fluorescence fluctuations by computing the photon counting histogram (Kask et al. 1999; Chirico et al. 2000; Muller et al. 2000). This is due to the fact that the dependence of the correlation function on the molecular brightness is brought by the first channel of the autocorrelation function $G(0)$ that is usually affected by a considerable uncertainty. On the other hand, the whole photon counting histogram shape depends critically on the molecular brightness and therefore its analysis can yield much more accurate results in determining the molecular brightness and the number of molecules per excitation volume. It is therefore interesting to test the simulation procedure and the model proposed here also for the computation of photon counting histogram. In order to do so we must take into account the Poisson statistics of the photodetector emission by weighing the fluorescence distribution $\mathscr{P}_\mathrm{F}(F)$ with a Poisson function as given by the Mandel-Wolf relation (Saleh 1978):

$$p(k) = \int_0^\infty \mathscr{P}_\mathrm{F}(\beta F)\frac{(\beta F)^k}{k!}\exp[-\beta F]\mathrm{d}F \tag{25}$$

where β is the quantum yield of the detector. In practice we compute the histogram of the simulated fluorescence and convert the previous equation to a discrete sum. The value of β should be obtained experimentally for each photodetector; in the following examples we have assumed $\beta \approx 1$. Typical results for these computations are shown in Fig. 5. The fluorescence histograms in Fig. 5a correspond to concentrations $C = 0.5$ nM and $C = 10$ nM and to the efficiency values $\beta = 1.6$ and $\beta = 0.3$, respectively. They are weighed over the Poisson function in order to obtain the photon counts histograms $p(k)$ reported in Fig. 5b. The statistical uncertainties on the histograms have been computed according to the relation (Chen et al. 1999):

$$\sigma(k) = \left[\frac{p(k)(1-p(k))}{M}\right]^{0.5} \tag{26}$$

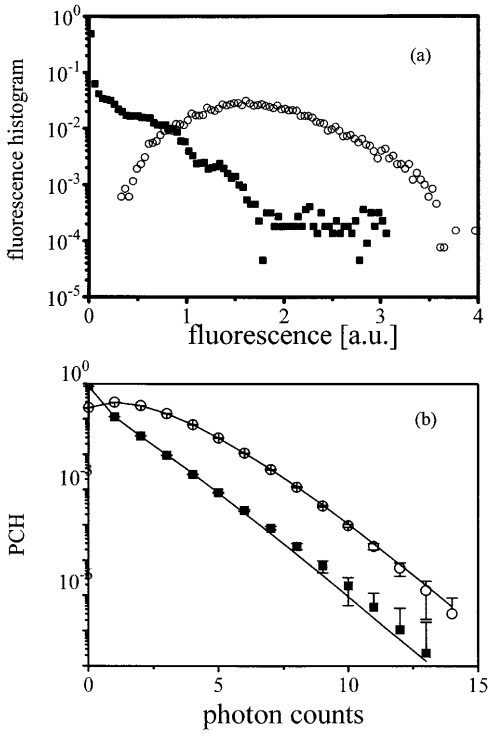

Fig. 5 **a** Histograms of the fluorescence computed for simulations corresponding to $C = 0.5$ nM (*filled squares*) and $C = 10$ nM (*open circles*). **b** Photon counting histograms computed for the two cases reported in **a** by assuming $\beta = 1.6$ (for $C = 0.5$ nM) and $\beta = 0.3$ (for $C = 10$ nM) in Eq. (25). The *solid lines* are the fit made according to the Eq. (27). The best fit values are $C_\mathrm{fit} = 0.45 \pm 0.1$ nM (for *filled squares*) and $C_\mathrm{fit} = 12 \pm 3$ nM (for *open circles*)

where we have assumed a total number of counts collected $M = 10^6$. The solid lines are the fit of the simulated photon counting histograms to the analytical relation developed by Chen et al. (1999):

$$p(k) = \sum_{n=0}^{\infty}\frac{\langle N\rangle^n \mathrm{e}^{-\langle N\rangle}}{n!}p^{(n)}(k, V_0, \beta)$$

$$p^{(n)}(k, V_0, \beta) = \frac{p^{(1)}(k, V_0, \beta) \otimes p^{(1)}(k, V_0, b) \otimes \cdots^{(1)}(k, V_0, \beta)}{n \text{ times}} \tag{27}$$

where V_0 is the integration volume and the single molecule photon counting histogram $p^{(1)}(k, V_0, \beta)$ is given for the 3-D Gaussian shape of the laser beam by Chen et al. (1999). The average number of molecules $\langle N\rangle$ per integration volume V_0 gives us the average best fit concentration $n_\mathrm{fit} = \langle N\rangle / V_0$. The analysis of the simulated histograms according to Eq. (27) is satisfactory for the two concentrations and gives best fit concentrations in good agreement with the simulated values, $n_\mathrm{fit} = 0.45 \pm 0.1$ nM and $n_\mathrm{fit} = 12 \pm 3$ nM, respectively. For the fluorescence efficiency we find $\beta = 0.3 \pm 0.1$ for the more concentrated solution and $\beta = 1.7 \pm 0.5$ for the more dilute solution, again in good agreement with the simulation values. The uncertainties in the best fit parameters are obtained by

simulating photon counting histograms on four subtrajectories for each simulation. This result indicates that the simulations of the photon counting histograms can be obtained from BD simulations.

We have further investigate the effect of the simulation statistics on the computation of the photon counting histogram by computing the histograms on subtrajectories of decreasing duration, finding that the simulation procedure gives very similar results even when we consider trajectories only 1/10 of the ones used for the computation of the autocorrelation functions or of the histograms reported in Fig. 5.

Scanning fluorescence correlation spectroscopy

In the scanning FCS technique, the beam is moved on a circular path centered in the middle of the cubic box, with radius A and period $T=2\pi/\omega$. The intensity distribution of the laser beam in the solution is therefore time dependent. The position of the center of the beam is displaced as a function of time by a scan vector:

$$\mathbf{r}_s(t) = A\cos(wt)\mathbf{i} + A\sin(wt)\mathbf{j} \tag{28}$$

This method (Berland et al. 1996) is used to avoid photobleaching (Eggeling et al. 1998) problems (which can arise if the sample has a slow diffusion) and to improve the determination of $G(0)$, which gives information on the average number of particles in the excitation volume.

The laser beam coordinates (x_L,y_L,z_L) are functions of time:

$$\begin{aligned} x_L &= L_{\text{box}}/2 + A\cos(wt) \\ y_L &= L_{\text{box}}/2 + A\sin(wt) \\ z_L &= L_{\text{box}}/2 \end{aligned} \tag{29}$$

The autocorrelation function is given in this case by the autocorrelation without scanning (Eq. 19) multiplied by a scanning factor (Berland et al. 1996), $S(\tau)$:

$$\begin{aligned} G_s(\tau) &= G(\tau)\cdot S(\tau) \\ &= \frac{\gamma}{\langle N\rangle}\frac{1}{\left(1+\frac{\tau}{\tau_d}\right)\left(1+\frac{\tau}{\tau_z}\right)^{1/2}}\exp\left[\frac{-4A^2(1-\cos(\omega t))}{\left(1+\frac{\tau}{\tau_d}\right)w_0^2}\right] \end{aligned} \tag{30}$$

This experimental method is based on the choice of a revolution period smaller than the diffusion time of the fluorescent probe. When a particle is found along the scanning path, it will be found also at the next revolution since it has not the time to diffuse away from the scanning path. Therefore we expect an echo signal after one period as well as after $2T$, $3T$, etc. However, the particle slowly diffuses away from the scanning path, so the height of these peaks decrease with time. Equation (30) describes this behavior analytically as developed by Berland et al. (1996).

On each of the BD simulations we have computed the scanning FCS correlation functions, obtaining decays similar to that of Fig. 6. These functions have been fit to Eq. (30) by leaving the average number of proteins per excitation volume, $\langle N\rangle$, the diffusion time, τ_d, and the scanning pulsation, ω, as free parameters. As in the non-scanning method, τ_z is assumed as $\tau_z=(z_0/w_0)^2\tau_d$. In all cases the whole decay of the correlation function has been successfully fit to Eq. (30), obtaining parameters that are in good agreement with the simulation values. For example, from the fit of the autocorrelation function in Fig. 6 we obtain $\tau_d=250$ μs and $\langle N\rangle=2.8$ that corresponds to $w_0=0.27$ μm and $c=28$ μg/L, in good agreement with the simulation parameters reported in the caption of Fig. 6.

Again, as in the non-scanning case, we verify that the simulation procedure works out properly representing τ_d as a function of w_0^2/D. The slope recovered from the linear fit is 0.24 ± 0.03, to be compared to the theoretical 0.25 value. The results obtained in our FCS and scanning FCS are composed together in Fig. 7. In the lower panel of Fig. 7, τ_d is plotted versus w_0^2/D and fit to a linear relation finding a slope of 0.25 ± 0.04, in good agreement with the theoretical value, 0.25. In Fig. 7, upper panel, we have compared the theoretical numerical concentration with the average number of particles within the excitation volume obtained from our simu-

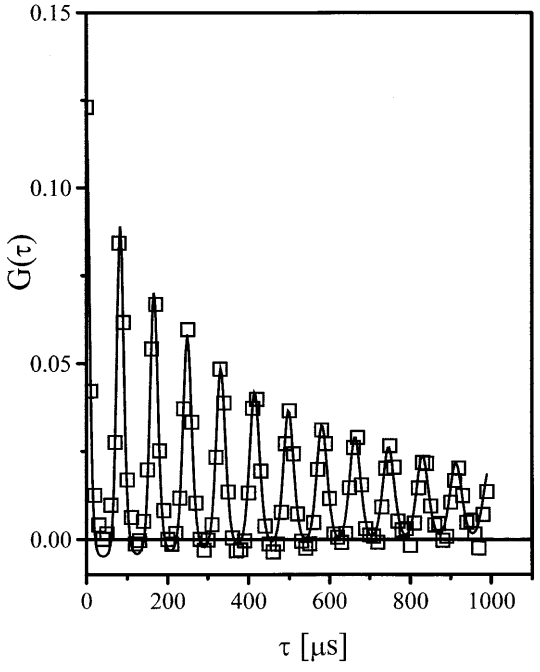

Fig. 6 Fluorescence autocorrelation function $G(\tau)$ simulated for the scanning case with scanning pulsation $\omega=75.7$ kHz and radius $A=0.24$ μm. The beam profile is characterized by $w_0=0.27$ μm, $z_0=1.35$ μm and $c=30$ μg/L. The best fit parameters are $\tau_d=250$ μs and $\langle N\rangle=2.8$

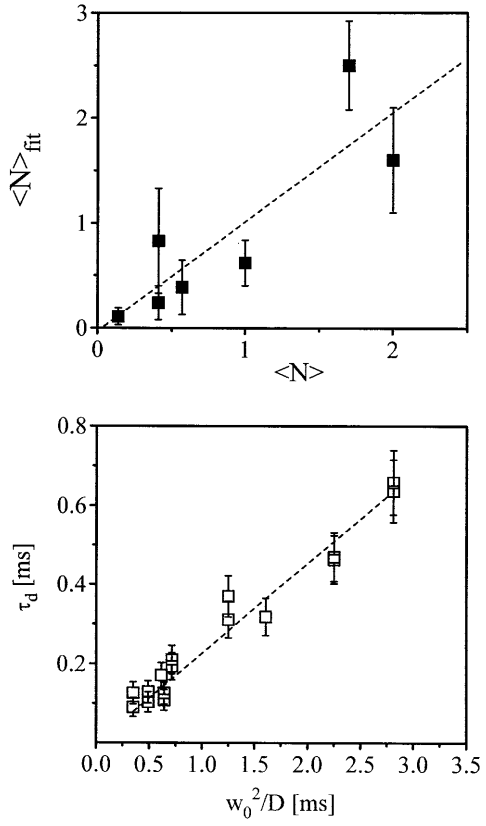

Fig. 7 Summary of the fitting of the autocorrelation functions for the scanning and non-scanning cases. The best fit values of the diffusion time are reported versus the ratio w_0^2/D in the *lower panel*. The linear fit reported in the plot corresponds to a slope 0.25 ± 0.04. In the *upper panel* the best fit values for the average number of proteins $\langle N \rangle_{\text{fit}}$ per excitation volume is reported versus the simulation value $\langle N \rangle$. The linear fit corresponds to a slope of 1.0 ± 0.15

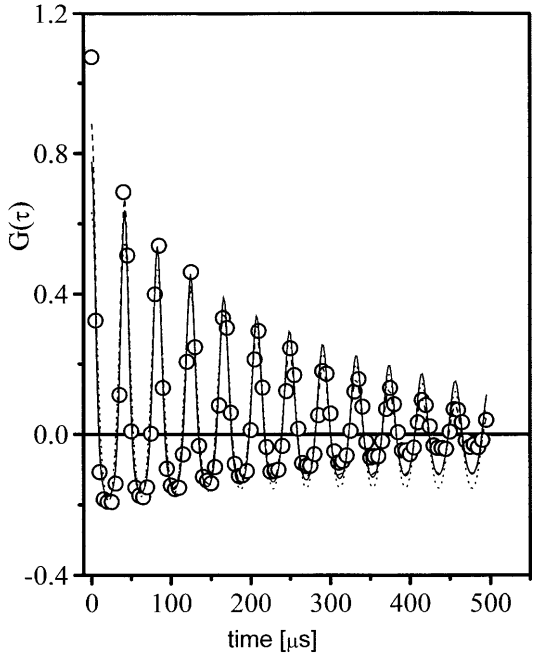

Fig. 8 Fluorescence autocorrelation function $G(\tau)$ simulated for the scanning case with $\omega = 151$ kHz and radius $A = 0.24$ μm. The beam profile is characterized by $w_0 = 0.35$ μm, $z_0 = 3$ μm and $C = 0.5$ nM. The best fit *solid line* corresponds to a number of molecules $\langle N \rangle = 0.38$ and has been obtained by keeping the diffusion time at $\tau_d = 250$ μs. The *dashed line* corresponds to $\langle N \rangle = 0.3$ with the diffusion time kept at $\tau_d = 170$ μs. The *dotted line* corresponds to $\langle N \rangle = 0.36$ with the diffusion time kept at $\tau_d = 430$ μs

lations. The initial value of the autocorrelation function ($G(0) = \gamma/\langle N \rangle$) gives the average number of molecules within the volume of sample illuminated by the laser beam. The slope of the fit has a value of 1.0 ± 0.15, very close to the expected behavior. The larger uncertainty in the value of $\langle N \rangle$ is probably due to the fact that the number of particles is very low, with consequent large fluctuations but low occupation times of the excitation volume. Much longer simulations should be run in order to reduce the uncertainty in this parameter.

Scanning FCS in highly diluted samples

We have computed the scanning autocorrelation functions for highly diluted solutions, corresponding to much less than one molecule per excitation volume. Also in this case we find a periodic behavior in phase with the scanning period, as it is evident from Fig. 8. The decay of the correlation functions resembles the one predicted by Eq. (30) and found for the simulations at higher concentration (see Fig. 6). However, we observe an anticorrelation effect particularly evident at short lag times, as shown by the autocorrelation function simulated for a $C = 0.5$ nM solution and plotted in Fig. 8. The fit of this decay to Eq. (30) is satisfactory only if we add a constant additive factor to the autocorrelation function. However, when the diffusion time is kept at the simulation value, $\tau_d \approx 430$ μs, the autocorrelation function is underestimated at short lag times and overestimated at long ones. The best fit value of the diffusion time, $\tau_d \approx 170$ μs, would correspond to a value of the beam waist, $w_0 \approx 0.22$ μm, sensibly smaller than the simulation value, $w_0 = 0.35$ μm. This indicates that Eq. (30) is not adequate to accurately describe the behavior of the autocorrelation functions of highly dilute solutions.

The anticorrelation effect is evident for lag times < 0.3 ms, i.e. for lag times of the order of the diffusion relaxation time. This effect disappears at higher concentrations (it is hardly visible in the function reported in Fig. 6) and may be interpreted as a non-uniform distribution of the molecules in the simulation box. For the simulation in Fig. 8 we have employed six molecules per simulation box whose volume was 20 fL, corresponding to a linear size of 2.7 μm. With such a low concentration it is very unlikely that the molecules are uniformly distributed over the box and therefore the fluorescence obtained by scanning the solution is, on the average, larger in one part of the scanning period than in the other. Let us imagine dividing the simulation volume into N sub-volumes, one for each of the N molecules. Then the probability to have

all the molecules in one sub-volume, a case that corresponds to the maximum inhomogeneity and therefore to the maximum anticorrelation, should scale as $\sim e^{-N}/(N+1)^{0.5}$. Therefore the larger is N, the smaller anticorrelation we should expect. If the diffusion of the fluorophores is such that in the simulation duration the molecules can exchange between different sub-volumes, then we should not expect a large dependence of the simulation output on the starting configuration of the system, as we have verified for the total simulation time of 210 ms (data not shown). In our case, the diffusion coefficient is $D = 71.4\ \mu m^2/s$ and the fluorophores displace on average $(Dt)^{0.5} \approx 3.8\ \mu m$ in the $t = 210$ ms of simulation that is larger than the linear size of each of the six simulation sub-volumes, $\sim 1.5\ \mu m$. Therefore in this case we expect that the inhomogeneous distribution of the fluorophores may be relevant and induce anticorrelation effects, although the simulation outputs are not much dependent on the starting random configuration. For macromolecules much larger than those simulated here, such as plasmid DNAs, this anticorrelation effect should be visible for longer times that are comparable with the diffusion time in the scanning area, $\sim \pi A^2$. In such cases, the translational and rotational diffusion of a single large macromolecule should affect the amount of the observed anticorrelations, that could then be used as a fingerprint of the molecular diffusive motions.

Conclusions

We have described a model for the Brownian dynamics simulation of fluorescence fluctuations arising from solutions of small uniformly fluorescent macromolecules. This algorithm can be useful to the study of small globular proteins and has been tested and applied here to the computation of fluorescence autocorrelation functions as well as photon counting histograms. The simulations of the scanning FCS for highly dilute solutions indicate the presence of a small but finite anticorrelation effect for lag times of the order of the diffusion time. This effect disappears at higher concentrations of the fluorophores and is probably due to the non-uniform occupation of the scanning area by the fluorescent molecules. We speculate here about the possibility to use this effect to study the diffusional motions of single large macromolecules. As a matter of fact, plasmid DNAs have elongated shapes with long axis 0.3–0.5 μm in length, comparable with the beam waist and to the scanning radius. In this case the anticorrelation effect should arise from the elongated shape of the DNA and the decay of the scanning autocorrelation function would be related to the tumbling rotational motion. We are currently investigating this possibility by performing Brownian dynamics simulations.

Acknowledgements This work has been partially supported by the 1999 funds of the Istituto Nazionale per la Fisica della Materia and by the 2000 funds of the Ministero della Ricerca Scientifica e Tecnologica, codice MM02273959. Marisa Huertas de la Torre was supported by a fellowship of the Fundación Séneca.

References

Allen MP, Tildesley DJ (1987) Computer simulation of liquids. Clarendon Press, Oxford

Berland K, So M, Chen Y, Mantulin WW, Gratton E (1996) Scanning two-photon fluctuation correlation spectroscopy – particle counting measurements for detection of molecular aggregation. Biophys J 71:410–420

Carrasco B, Garcia de la Torre JG, Zipper P (1999) Calculation of hydrodynamic properties of macromolecular bead models with overlapping spheres. Eur Biophys J 28:510–515

Chen Y, Muller JD, So PTC, Gratton E (1999). The photon counting histogram in fluorescence fluctuation spectroscopy. Biophys J 77:553–567

Chirico G, Bettati S, Mozzarelli A, Chen Y, Müller JD, Gratton E (2000) Molecular heterogeneity of *O*-acetylserine sulfhydrylase by two-photon excited fluorescence fluctuation spectroscopy. Biophys J (in press)

Dhont JKG (1996) An introduction of dynamics of colloids. In: Möbius D, Miller R (eds) Studies in interface science. Elsevier, Amsterdam, pp 1–13

Dickinson E, Allison SA, McCammon JA (1985) Brownian dynamics with rotation-translation coupling. J Chem Soc Faraday Trans 2 81:591–601

Eggeling C, Widengren J, Rigler R, Seidel CAM (1998) Photobleaching of fluorescent dyes under conditions used for single molecule detection: evidence of two-step photolysis. Anal Chem 70:2651–2659

Ermak DL, McCammon JA (1978) Brownian dynamics with hydrodynamic interactions. J Chem Phys 69:1352–1360

Iniesta A, Garcia de la Torre J (1990) A second-order algorithm for the simulation of the Brownian dynamics of macromolecular models. J Chem Phys 92:2015–2018

Kask P, Palo K, Ullmann D, Gall K (1999) Fluorescence-intensity distribution analysis and its application in biomolecular detection technology. Proc Natl Acad Sci USA 96:13756–13761

Kask P, Palo K, Fay N, Brand L, Mets U, Ullmann D, Jungmann J, Pschorr J, Gall K (2000) Two-dimensional fluorescence intensity distribution analysis: theory and applications. Biophys J 78:1703–1713

Koppel DE (1974) Statistical accuracy in fluorescence correlation spectroscopy. Phys Rev A 10:1938–1945

Muller JD, Chen Y, Gratton E (2000) Resolving heterogeneity on the single molecular level with the photon-counting histogram. Biophys J 78:474–486

Quian H (1990) On the statistics of fluorescence correlation spectroscopy. Biophys Chem 38:49–57

Quian H, Elson EL (1990) Distribution of molecular aggregation by analysis of fluctuation moments. Proc Natl Acad Sci USA 87:5479–5483

Rigler R, Mets U, Windegren J, Kask P (1993) Fluorescence correlation spectroscopy with high count rate and low background: analysis of translational diffusion. Eur Biopys J 22:169–175

Rotne J, Prager S (1969) Variational treatment of hydrodynamic interaction on polymer. J Chem Phys 50:4831–4837

Saleh B (1978) Photoelectron statistics, with applications to spectroscopy and optical communications. Springer, Berlin Heidelberg New York, pp 160–248

Schwille P, Bieschke J, Oehlenschlager F (1997) Kinetic investigations by fluorescence correlation spectroscopy – the analytical and diagnostic potential of diffusion studies. Biophys Chem 66:211–228

So PTC, French T, Yu WM, Berland KM, Dong CY, Gratton E (1995) Time-resolved fluorescence microscopy using two-photon excitation. Bioimaging 3:49–63

Widengren J, Mets Ü, Rigler R (1995) Fluorescence correlation spectroscopy of triplet states in solution: a theoretical and experimental study. J Phys Chem 99:13368–13379

Wilson T (1990) Optical aspects of confocal microscopy. In: Wilson T (ed) Confocal microscopy. Academic Press, London, pp 1–60

Yamakawa H (1970) Transport properties of polymer chains in dilute solutions. Hydrodynamic interaction. J Chem Phys 53:436–443

Zipper P, Durchschlag H (1997) Calculation of hydrodynamic parameters of proteins from crystallographic data using multi-body approaches. Prog Colloid Polym Sci 107:43–57